

Acoustic oscillations in the SDSS Luminous Red Galaxy sample power spectrum

G. Hütsi

Max-Planck-Institut für Astrophysik, Karl-Schwarzschild-Str. 1, 86740 Garching bei München, Germany

Received / Accepted

Abstract. We calculate the redshift-space power spectrum of the Sloan Digital Sky Survey (SDSS) Luminous Red Galaxy (LRG) sample, finding evidence for a full series of acoustic features down to the scales of $\sim 0.25 h \text{ Mpc}^{-1}$. This corresponds up to the 9. peak in the CMB angular power spectrum. The acoustic scale derived, $(107.8 \pm 4.3) h^{-1} \text{ Mpc}$ ($k \lesssim 0.2 h \text{ Mpc}^{-1}$), agrees very well with the “concordance” model prediction and also with the one determined via the analysis of the spatial two-point correlation function by Eisenstein et al. (2005). This is not only an independent confirmation of Eisenstein et al. (2005) results made with different methods and software but also, according to our knowledge, the first determination of the power spectrum of the SDSS LRG sample. By calculating the two-point correlation function using the smooth cubic spline model fitted to the observed bandpowers and comparing with the results of the direct determination we demonstrate the consistency of our results.

Key words. large-scale structure of Universe

1. Introduction

In the beginning of 1970’s it was already realized that acoustic waves in the tightly coupled baryon-photon fluid prior to the epoch of recombination will lead to the characteristic maxima and minima in the post-recombination matter power spectrum. The same mechanism is also responsible for the prominent peak structure in the CMB angular power spectrum (Sunyaev & Zeldovich 1970; Peebles & Yu 1970; Doroshkevich et al. 1978). The scale of these features reflects the size of the sound horizon, which itself is fully determined given the physical densities $\Omega_b h^2$ and $\Omega_m h^2$. The acoustic horizon can be calibrated using the CMB data, thus turning it into a standard ruler which can be used to carry out standard cosmological tests. For example, if we are able to measure the redshift and angular intervals corresponding to the physically known acoustic scale in the matter power spectrum at a range of redshifts, we can immediately find angular diameter distance d_A and Hubble parameter H as a function of redshift. Having good knowledge of these dependencies allows us to put constraints on the properties of the dark energy. To carry out this project one needs a tracer population of objects whose clustering properties with respect to the underlying matter distribution is reasonably well understood. There have been several works discussing the usage of galaxies (Blake & Glazebrook 2003; Hu & Haiman 2003; Linder 2003; Seo & Eisenstein 2003) and clusters of galaxies (Hu & Haiman 2003; Majumdar & Mohr 2004; Hütsi 2005) for this purpose. What is most important is that already currently

existing galaxy redshift surveys have lead to the detection of acoustic features in the spatial distribution of galaxies, this way providing clearest support for the standard gravitational instability picture of the cosmic structure formation. In the paper by Eisenstein et al. (2005) the detection of the acoustic “bump” in the two-point redshift-space correlation function of the SDSS¹ LRG sample is announced. The discovery of similar features in the power spectrum of 2dF² galaxies is presented in Cole et al. (2005). These results clearly demonstrate the great promise of the future dedicated galaxy redshift surveys like K.A.O.S.³ Similarly, useful measurements of the acoustic scale can be hoped by the planned SZ cluster surveys like the ones carried out by the PLANCK Surveyor⁴ spacecraft and SPT⁵ (Hütsi 2005) and also with a large future photometric redshift surveys (Blake & Bridle 2005). In this paper we calculate the redshift-space power spectrum of the SDSS LRG sample finding evidence for the acoustic oscillations down to the scales of $\sim 0.25 h \text{ Mpc}^{-1}$, which effectively correspond up to the 9. peak in the CMB angular power spectrum. These scales in the CMB are very strongly damped due to the finite width of the last-scattering surface and also due to the Silk damping (Silk 1968). Also, at those scales the secondary CMB anisotropies (mostly thermal Sunyaev-Zeldovich effect (Sunyaev & Zeldovich 1972, 1980)) start to dominate over the primary signal. On the other hand, features in the matter power spectrum, although being

¹ <http://www.sdss.org/>

² <http://www.mso.anu.edu.au/2dFGRS/>

³ <http://www.noao.edu/kaos/>

⁴ <http://astro.estec.esa.nl/Planck>

⁵ <http://astro.uchicago.edu/spt>

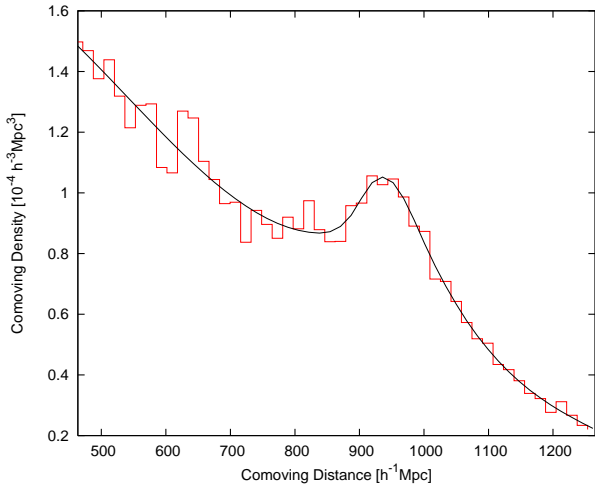


Fig. 1. Comoving number density of galaxies as a function of comoving distance. Smooth solid line shows a cubic spline fit to the number density estimated for 50 discrete radial bins.

small ($\sim 5\%$ fluctuations), are preserved by the linear evolution and so opening up the way to probe acoustic phenomena at scales smaller than the ones accessible for the CMB studies.

The paper is structured as follows. In Sec. 2 we describe the dataset to be analysed, Sec. 3 presents the method of the power spectrum calculation. The main results of this work are given in Sec. 4 and finally we conclude with Sec. 5.

2. Data

We analyze the publicly available data from the SDSS Data Release 3 (Abazajian et al. 2005). Specifically, we carry out our power spectrum measurements using the subset of the SDSS spectroscopic sample known as the Luminous Red Galaxy (LRG) sample. The LRG selection algorithm (Eisenstein et al. 2001) selects ~ 12 galaxies per square degree meeting specific colour and magnitude criteria⁶. The resulting set of galaxies consists mostly of an early types populating dense cluster environments and as such are significantly biased (bias factor $b \sim 2$) with respect to the underlying matter distribution. The selection method is very effective producing a galaxy sample with a reasonably high density up to the redshift of $z \sim 0.5$.

Since the selection criteria are very complicated, involving both cuts in magnitude and in color, and also due to the steepness of the luminosity function the usual method of using only the luminosity function to determine radial selection function does not work here (Zehavi et al. 2005). Here we simply build the radial selection function as a smooth spline fit to the number density profile as shown in Fig. 1. To calculate distances we choose the cosmological parameters as given by the WMAP⁷ ‘concordance’ model (Spergel et al. 2003). Unfortunately we could not find the data describing properly the survey geom-

⁶ For the exact details of the selection criteria see Eisenstein et al. (2001)

⁷ <http://lambda.gsfc.nasa.gov/product/map/>

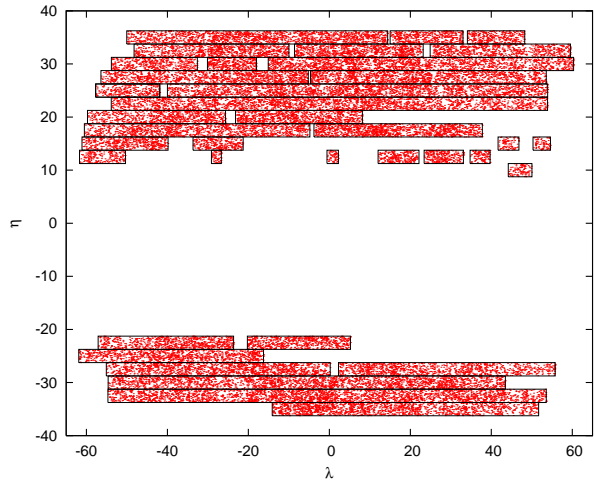


Fig. 2. Angular distribution of galaxies given in the SDSS survey coordinates (λ, η) . The survey mask is shown with solid lines.

etry⁸ and so were forced to build the angular survey masks using the galaxy data itself. As the number density of galaxies in the sample is rather high, one can determine relatively accurately the beginning, ending and also possible gaps in the scan stripes. The angular distribution of the galaxies and also the boundaries of the survey mask built in the above mentioned way is shown in Fig. 2. Here the angular positions are plotted using the so-called survey coordinate system of the SDSS⁹. We apply lower and upper redshift cutoffs of 0.16 and 0.47 as also done in Eisenstein et al. (2005). In the analysis presented in this paper we have excluded the three southern stripes since these just make the survey window more anisotropic. We have also carried out calculations by including these stripes, finding out that the amount of additional information they provide is rather minor. Due to the very small sky coverage we have not used the data in slices 15, 42 and 43. So in total the analyzed galaxy sample covers $0.57 h^{-3} \text{ Gpc}^3$ over 2920 square degrees on the sky and contains 37,998 galaxies.

3. Power spectrum calculation

We calculate the power spectrum using a direct Fourier method as described in Feldman et al. (1994) (FKP). Strictly speaking, power spectra determined this way are the so-called pseudo spectra, meaning that the estimates derived are convolved with a survey window. Since in the case of the analysed LRG sample the volume covered is very large, reaching $0.57 h^{-3} \text{ Gpc}^3$, and also the survey volume has relatively large dimensions along all perpendicular directions, the correlations in the Fourier space are rather compact. In general FKP estimator is working fine on intermediate scales and in the case the power spectrum binning is wide enough. More precisely, one can say that this estimator is fine for wavenumbers k and power spectrum bins Δk larger than the width of the survey window function $|W_{\mathbf{k}}|^2$, where $W_{\mathbf{k}}$

⁸ The data related to the geometry seemed to be newer than the actual galaxy data.

⁹ The transformations between various coordinate systems used by the SDSS are given e.g. in Stoughton et al. (2002).

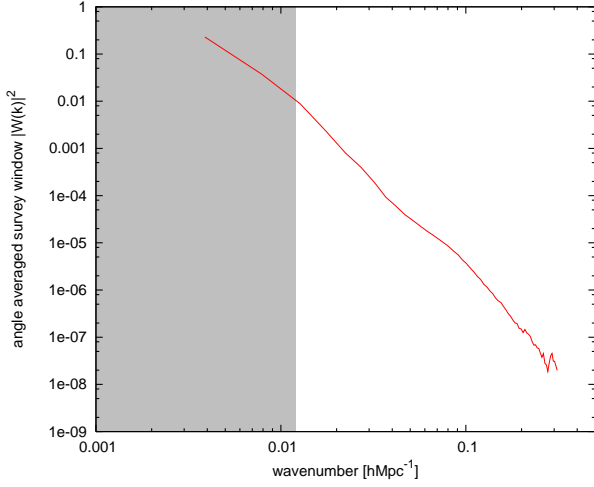


Fig. 3. Angle-averaged survey window $|W(k)|^2$. The gray shaded area shows the region where the window is larger than 1% of its maximum value.

is the Fourier transform of the product of the survey mask and radial selection function. The angle average of this quantity is shown in Fig. 3, where we have also marked with a gray shaded stripe the scale where it is larger than 1% of its maximum value. This scale should serve as a rather conservative estimate of the effective window width. In the following we make sure that the power spectrum bins are chosen to be large enough so that the above discussed criteria are satisfied. To speed up the calculations of the power spectrum we make use of the Fast Fourier Transforms (FFTs), meaning that we need to build density field on a grid first. We use 512^3 grid with a Triangular Shaped Cloud (TSC) mass assignment scheme (Hockney & Eastwood 1988). Very briefly the steps involved in calculating the power spectrum are as follows:

1. determination of the survey selection function (including the survey geometry) and mean underlying number density \bar{n} ,
2. calculation of the overdensity field on a grid using TSC mass assignment scheme,
3. Fourier transformation of the gridded density field,
4. calculation of the raw 3D power spectrum,
5. subtraction of the shot noise component from the raw spectrum,
6. isotropization of the shot noise corrected 3D spectrum i.e. averaging over k -space shells,
7. application of the normalization correction due to selection effects,
8. deconvolving the smearing effect of the TSC mass assignment.

More detailed description of our computational method with the results of application to a multitude of test problems can be found in Hütsi (2005). The power spectrum errors are estimated using the simple “mode counting” result of FKP (see also Tegmark et al. (1998)):

$$\frac{\Delta P}{P} = \sqrt{\frac{2}{V_{\text{eff}} V_k}},$$

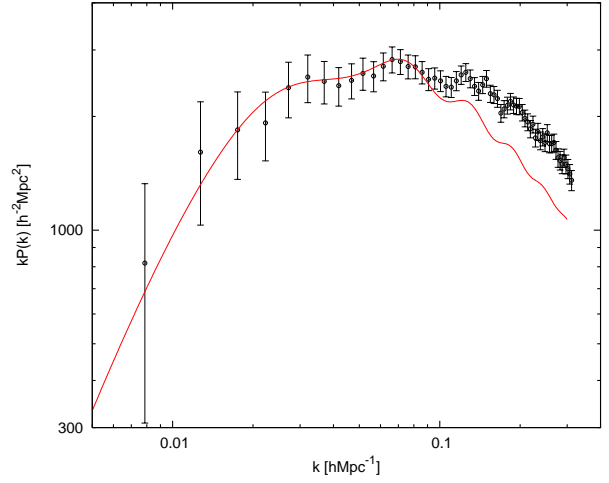


Fig. 4. Power spectrum of the SDSS LRG sample with the bin width $\Delta k \sim 0.005 h \text{ Mpc}^{-1}$. The solid line shows the linearly evolved matter power spectrum for the “concordance” cosmological model multiplied by the square of the bias parameter $b = 1.95$.

where $V_k = 4\pi k^2 \Delta k / (2\pi)^3$ is the volume of the k -space shell and V_{eff} is the effective volume given by:

$$V_{\text{eff}} = \frac{\left[\int w^2(z) \frac{dV_c}{dz} dz \right]^2}{\int w^4(z) \left[1 + \frac{1}{\bar{n}(z)P} \right]^2 \frac{dV_c}{dz} dz}.$$

Here $\bar{n}(z)$ is the mean number density of objects at redshift z , dV_c is a comoving volume element and the weight function:

$$w(z) \propto \begin{cases} \text{const} & \text{for volume weighting} \\ \bar{n}(z) & \text{for number weighting} \\ \frac{\bar{n}(z)}{1 + \bar{n}(z)P} & \text{for an optimal FKP weighting.} \end{cases}$$

In the following we use the FKP weight function, although due to the rather high number density and clustering strength of the sample the pure volume weighting is giving almost identical results.

4. Results

In this section we present the main results of this work. In Fig. 4 we show the redshift-space power spectrum of the above described SDSS LRG sample. We see that the power spectrum agrees remarkably well with the linearly evolved “concordance” model spectrum (shown with a solid line) down to the scales of $\sim 0.1 h \text{ Mpc}^{-1}$, beyond which the non-linear evolution starts to boost the power. Here the bin width $\Delta k \sim 0.005 h \text{ Mpc}^{-1}$ is probably too narrow for the bins to be independent of each other. In Fig. 5 we have increased the bin width up to $\sim 0.02 h \text{ Mpc}^{-1}$ and built a smooth cubic spline curve through the data points, revealing clear hints for the oscillatory behaviour of the spectrum. In addition we have plotted the same linearly evolved theoretical power spectrum as in the previous figure as well as the spectrum of a similar model but with a zero baryon content (shown by the dashed curve without any oscillatory behaviour). In order to display the detected fluctuations in a more clear manner we have fitted a smooth

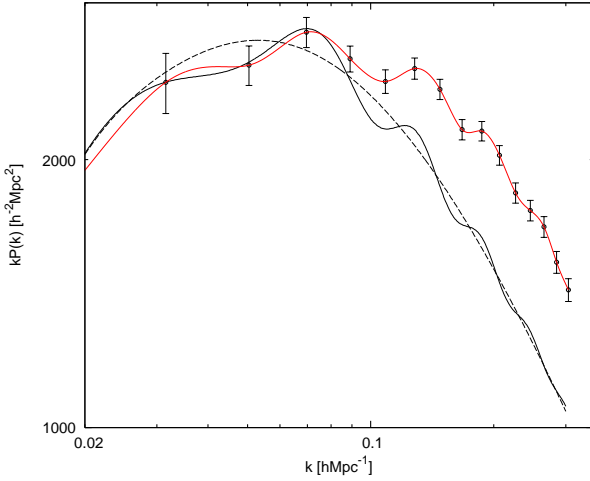


Fig. 5. Power spectrum of the SDSS LRG sample with the bin width $\Delta k \sim 0.02 h \text{Mpc}^{-1}$. The upper solid line shows the smooth cubic spline model built through the data points, whereas the lower one corresponds to the same theoretical linearly evolved model as in Fig. 4. The dashed line displays the model with zero baryon content.

function in the form of a second order polynomial in log–log coordinates to the observed bandpowers. In Fig. 6 we plot the same spectra as in the previous figure¹⁰ after dividing by this smooth function. The light gray shaded stripe shows the effective width of the survey window as described above.

It would be interesting to study how these oscillations in the power spectrum translate to the peak in the two-point correlation function discovered by Eisenstein et al. (2005). For this purpose we use the cubic spline model described above and extend it outside of the observed range by smoothly joining it to the power spectrum of the “concordance” model. The correlation function is now simply calculated as a Fourier transform of the power spectrum. To study the significance of the features at higher wavenumbers we have calculated correlation functions for several models that have oscillations “switched off” at various scales. The spectra of these models are shown in Fig. 7, where for the sake of clarity we have introduced slight vertical shifts between the curves so that the scales where the transition to the featureless spectrum takes place are easily visible. The corresponding correlation functions are given in Fig. 8. As expected, we see how the peak in the correlation function is getting broader and also decreasing in amplitude as we erase more features in the power spectrum. This clearly demonstrates the importance of many of the up-downs in the power spectrum to produce a relatively sharp feature in the two-point correlation function. Additionally, in this figure the circles with errorbars show the correlation function determined straight from the data using the edge-corrected estimator given by Landy & Szalay (1993):

$$\xi(r) = \frac{DD - 2DR + RR}{RR},$$

which has minimal variance for a Poisson process. Here DD, DR and RR represent the respective normalized data-data, data-

¹⁰ With the only exception that we have not plotted a spectrum for a model with zero baryon content.

random and random-random pair counts in a given distance range. Random catalogs were generated with 25 times the number of objects in the main catalog. The displayed errorbars are the simple Poissonian ones multiplied by the factor of 2. Since our aim here is not to perform any detailed correlation function study, this approximate treatment of errors, where one simply multiplies the Poissonian errorbars (which underestimate true errors) by some “fudge” factor in the range 1.5 – 2.5 (see e.g. Mo et al. (1992); Martinez et al. (1993)), should be well justified. The crosses with the dashed-line errorbars show the two-point function as determined by Eisenstein et al. (2005). We see that in general our results agree very well with their calculations.

To estimate the period of oscillations we calculate the periodogram $P_X(\omega)$ as described in Horne & Baliunas (1986):

$$P_X(\omega) = \frac{1}{2} \left\{ \frac{\left[\sum_{j=1}^{N_0} X(t_j) \cos \omega(t_j - \tau) \right]^2}{\sum_{j=1}^{N_0} \cos^2 \omega(t_j - \tau)} + \frac{\left[\sum_{j=1}^{N_0} X(t_j) \sin \omega(t_j - \tau) \right]^2}{\sum_{j=1}^{N_0} \sin^2 \omega(t_j - \tau)} \right\},$$

where

$$\tan(2\omega\tau) = \frac{\sum_{j=1}^{N_0} \sin 2\omega t_j}{\sum_{j=1}^{N_0} \cos 2\omega t_j}$$

and $X(t_j)$ represents a time series with N_0 data points. We calculate the frequency of oscillations for two different cases: (i) points with wavenumbers up to $k \sim 0.2 h \text{Mpc}^{-1}$ (first 10 data points), (ii) all 15 data points. The periodograms normalized by the total variance $P_N(\omega) = P_X(\omega)/\sigma^2$ are shown in Fig. 9, where the solid line corresponds to the case (i). The uncertainty in the oscillation frequency is estimated as (Horne & Baliunas 1986):

$$\sigma_\omega = \frac{3\pi\sigma_N}{2\sqrt{N_0}TA},$$

where σ_N is the variance of the residuals after the signal has been subtracted, T is the total length of the data set and A is the amplitude of the signal.

The acoustic scales measured in the above described manner are $(107.8 \pm 4.3) h^{-1} \text{Mpc}$ and $(101.8 \pm 3.2) h^{-1} \text{Mpc}$ for the cases (i) and (ii), respectively. These should be compared with the best-fit WMAP “concordance” model prediction of $106.5 h^{-1} \text{Mpc}$. It is worth pointing out that the acoustic scale in the matter power spectrum is slightly larger than the corresponding scale in the CMB angular power spectrum due to the fact that acoustic waves do not stall completely at the epoch of decoupling, but keep on moving (although with a strongly reduced speed) up to the redshift $z \sim 100$ (the so-called drag-epoch).

5. Discussion and Conclusions

In this paper we have calculated the redshift-space power spectrum of the SDSS LRG sample, finding evidence for a series of

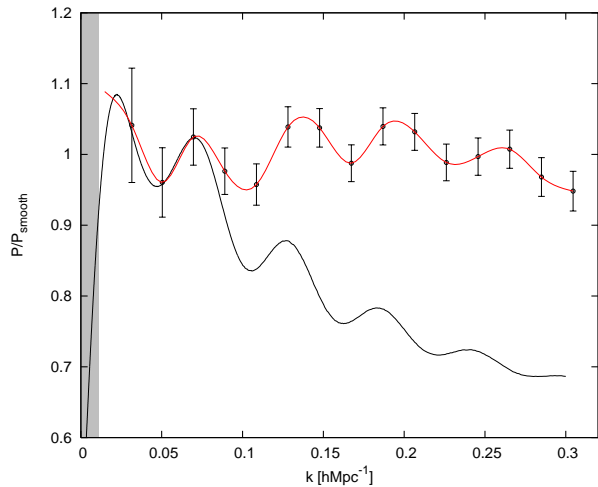


Fig. 6. The same spectra as in Fig. 5, except divided by the best fitting parabola in log-log coordinates, revealing clearly the oscillatory behaviour. The gray shaded stripe shows the effective width of the survey window as described in the main text.

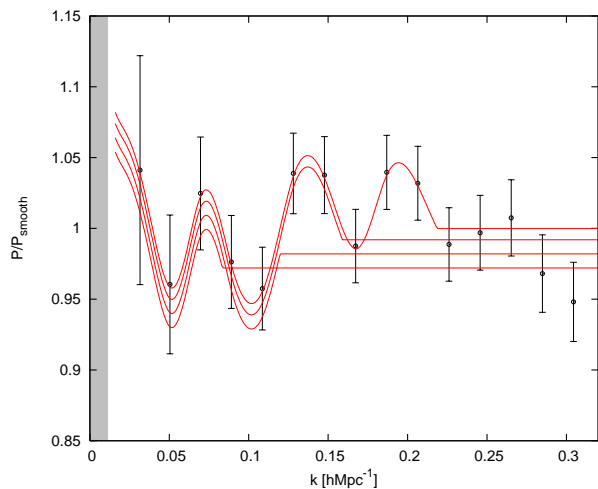


Fig. 7. Model spectra used to study the significance of the oscillatory features. Slight vertical shifts have been introduced in order to show clearly the locations of the transition scales applied.

acoustic features down to the scales of $\sim 0.25 h \text{ Mpc}^{-1}$. Using the obtained power spectrum we predict the shape of the spatial two-point correlation function, which agrees very well with the one obtained directly from the data. Also, the directly calculated correlation function is consistent with the results obtained by Eisenstein et al. (2005). We have made no attempts to put constraints on the cosmological parameters, rather we have assumed in our analysis the “concordance” cosmological model. The derived acoustic scale $(107.8 \pm 4.3) h^{-1} \text{ Mpc}$ ($k \lesssim 0.2 h \text{ Mpc}^{-1}$) agrees well with the best-fit WMAP “concordance” model prediction of $106.5 h^{-1} \text{ Mpc}$. Using all the data down to the wavenumbers $k \sim 0.3 h \text{ Mpc}^{-1}$, the obtained acoustic scale is somewhat shorter, which might be due to the nonlinear effects (transfer of power from large to small scales).

The existence of the baryonic features in the galaxy power spectrum is very important, allowing one (in principle) to obtain Hubble parameter H and angular diameter distance d_A as

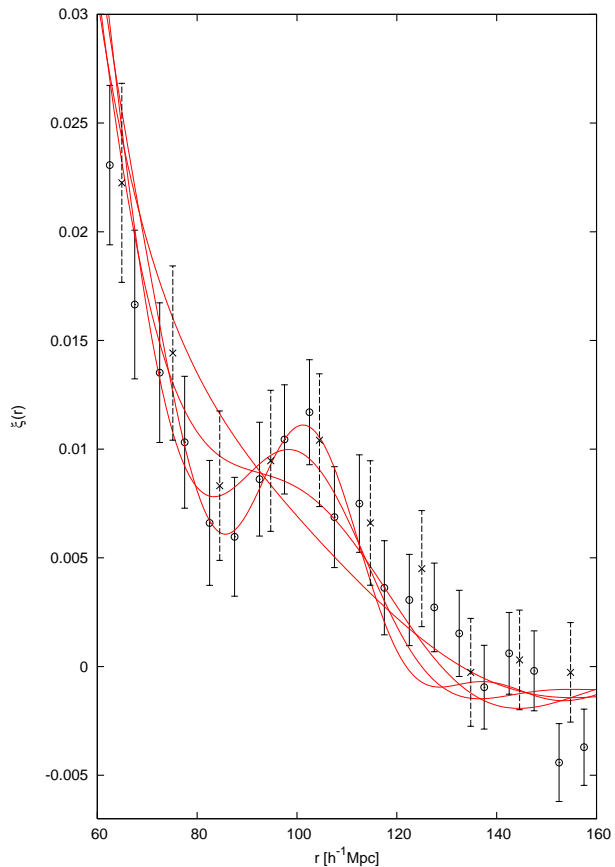


Fig. 8. Two-point correlation functions corresponding to the models shown in Fig. 7. The circles display the correlation function as determined directly from the data. The plotted errorbars are simply 2 times the Poissonian errors. And finally, the crosses with dashed errorbars show the correlation function found by Eisenstein et al. (2005).

a function of redshift, this way opening up a possibility to constrain properties of the dark energy (Hu & Haiman 2003). The currently existing biggest redshift surveys, which are still quite shallow, do not yet provide enough information to carry out this project fully. On the other hand, it is extremely encouraging that even with the current generation of redshift surveys we are already able to see the traces of acoustic oscillations in the galaxy power spectrum, showing the great promise for the dedicated future surveys like K.A.O.S. We have seen that acoustic features seem to survive at mildly nonlinear scales ($k \gtrsim 0.1 h \text{ Mpc}^{-1}$), which is in agreement with the results of the recent N-body simulations (Springel et al. 2005; Seo & Eisenstein 2005). In order to fully exploit available information one needs a complete understanding of how nonlinear effects influence these features. Nonlinear bias and redshift space distortions also add extra complications. In general redshift-space distortions, biasing and nonlinear evolution do not create any oscillatory modulation in the power spectrum and so acoustic features should be readily observable. On the other hand, only the effects that change the amplitude of the spectrum (e.g. redshift-space distortions on large scales) are easily factored out, but the ones involving stretching/compressing of the spatial scales do start to interfere with the cosmological distor-

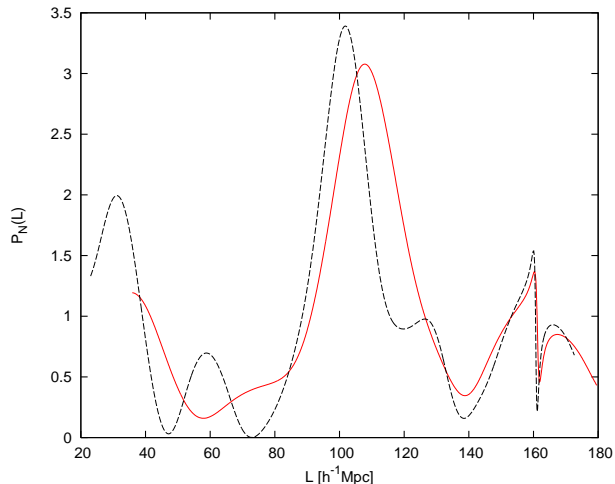


Fig. 9. The total variance normalized periodograms $P_N(L) = P_X(L)/\sigma^2$ for (i) power spectrum points with wavenumbers up to $k \sim 0.2 h \text{Mpc}^{-1}$ (first 10 data points), (ii) all 15 data points. Case (i) is shown with a solid line.

tions and so inhibit our ability to draw conclusions about the underlying cosmological model. So far there have been only a few works studying these important issues (e.g. Springel et al. (2005); Seo & Eisenstein (2005); White (2005)) and probably it is fair to say that currently we really do not have a full theoretical description of them. This is also the reason why we have not tried to carry out any parameter estimation in this paper.

The bare existence of the baryonic oscillations in the galaxy power spectrum tells us something important about the underlying cosmological model and the mechanism of the structure formation. First, it confirms the generic picture of the gravitational instability theory where the structure in the Universe is believed to be formed by the gravitational amplification of the small perturbations in the early Universe. Under the linear gravitational evolution all the density fluctuation modes evolve independently i.e. all the features in the power spectrum will be preserved. And certainly, we are able to identify features in the low redshift galaxy power spectrum that correspond to the fluctuations seen in the CMB angular power spectrum (which probes redshifts $z \sim 1100$), providing strong support for the above described standard picture of the structure formation. Actually, we can also probe scales that are inaccessible for the CMB studies due to the strong damping effects and steeply rising influence of the secondary anisotropies, reaching effectively the wavenumbers that correspond to the 8. – 9. peaks in the CMB angular power spectrum. Second, the ability to observe baryonic features in the low redshift galaxy power spectrum demands rather high baryonic to total matter density ratio. In Blanchard et al. (2003) it has been shown that it is possible to fit a large body of observational data with an Einstein–de Sitter type model if one adopts low value for the Hubble parameter and relaxes the usual assumptions about the single power law initial spectrum. In the light of the results obtained in our paper these models are certainly disfavored due to the fact that the high dark matter density completely damps the baryonic features. And finally, purely baryonic models are also ruled out

since for them the expected acoustic scale would be roughly two times larger than observed here¹¹. So the data seems to demand a weakly interacting nonrelativistic matter component and all the models that try to replace this dark matter component with something else e.g. modifying the laws of gravity might have hard time to fit these new observational constraints.

Acknowledgements. I thank Rashid Sunyaev for valuable comments on the manuscript. I am very grateful to the support provided through the European Community’s Human Potential Programme under contract HPRN-CT-2002-00124, CMBNET.

Funding for the creation and distribution of the SDSS Archive has been provided by the Alfred P. Sloan Foundation, the Participating Institutions, the National Aeronautics and Space Administration, the National Science Foundation, the U.S. Department of Energy, the Japanese Monbukagakusho, and the Max Planck Society. The SDSS Web site is <http://www.sdss.org/>.

The SDSS is managed by the Astrophysical Research Consortium (ARC) for the Participating Institutions. The Participating Institutions are The University of Chicago, Fermilab, the Institute for Advanced Study, the Japan Participation Group, The Johns Hopkins University, the Korean Scientist Group, Los Alamos National Laboratory, the Max-Planck-Institute for Astronomy (MPIA), the Max-Planck-Institute for Astrophysics (MPA), New Mexico State University, University of Pittsburgh, University of Portsmouth, Princeton University, the United States Naval Observatory, and the University of Washington.

References

- Abazajian, K., Adelman-McCarthy, J. K., Agüeros, M. A., et al. 2005, *AJ*, 129, 1755
 Blake, C. & Bridle, S. 2005, *MNRAS*, submitted; astro-ph/0411713
 Blake, C. & Glazebrook, K. 2003, *ApJ*, 594, 665
 Blanchard, A., Douspis, M., Rowan-Robinson, M., & Sarkar, S. 2003, *A&A*, 412, 35
 Cole, S., Percival, W. J., Peacock, J. A., et al. 2005, *MNRAS*, submitted; astro-ph/0501174
 Doroshkevich, A. G., Zel’Dovich, Y. B., & Syunyaev, R. A. 1978, *Soviet Astronomy*, 22, 523
 Eisenstein, D. J., Annis, J., Gunn, J. E., et al. 2001, *AJ*, 122, 2267
 Eisenstein, D. J., Zehavi, I., Hogg, D. W., et al. 2005, *ApJ*, submitted; astro-ph/0501171
 Feldman, H. A., Kaiser, N., & Peacock, J. A. 1994, *ApJ*, 426, 23
 Hockney, R. W. & Eastwood, J. W. 1988, *Computer simulation using particles* (Bristol: Hilger, 1988)
 Horne, J. H. & Baliunas, S. L. 1986, *ApJ*, 302, 757
 Hu, W. & Haiman, Z. 2003, *Phys. Rev. D*, 68, 063004
 Hütsi, G. 2005, *A&A*, submitted; astro-ph/0505441
 Landy, S. D. & Szalay, A. S. 1993, *ApJ*, 412, 64
 Linder, E. V. 2003, *Phys. Rev. D*, 68, 083504
 Majumdar, S. & Mohr, J. J. 2004, *ApJ*, 613, 41
 Martinez, V. J., Portilla, M., Jones, B. J. T., & Paredes, S. 1993, *A&A*, 280, 5
 Mo, H. J., Jing, Y. P., & Boerner, G. 1992, *ApJ*, 392, 452
 Peebles, P. J. E. & Yu, J. T. 1970, *ApJ*, 162, 815
 Seo, H. & Eisenstein, D. J. 2003, *ApJ*, 598, 720
 Seo, H. & Eisenstein, D. J. 2005, *ApJ*, accepted; astro-ph/0507338
 Silk, J. 1968, *ApJ*, 151, 459
 Spergel, D. N., Verde, L., Peiris, H. V., et al. 2003, *ApJS*, 148, 175

¹¹ For a clear discussion of this see Daniel Eisenstein’s home page <http://cmb.as.arizona.edu/~eisenste/acousticpeak/>

- Springel, V., White, S. D. M., Jenkins, A., et al. 2005, *Nature*, 435, 629
- Stoughton, C., Lupton, R. H., Bernardi, M., et al. 2002, *AJ*, 123, 485
- Sunyaev, R. A. & Zeldovich, I. B. 1980, *ARA&A*, 18, 537
- Sunyaev, R. A. & Zeldovich, Y. B. 1970, *Ap&SS*, 7, 3
- Sunyaev, R. A. & Zeldovich, Y. B. 1972, *Comments on Astrophysics and Space Physics*, 4, 173
- Tegmark, M., Hamilton, A. J. S., Strauss, M. A., Vogeley, M. S., & Szalay, A. S. 1998, *ApJ*, 499, 555
- White, M. 2005, [astro-ph/0507307](#)
- Zehavi, I., Eisenstein, D. J., Nichol, R. C., et al. 2005, *ApJ*, 621, 22